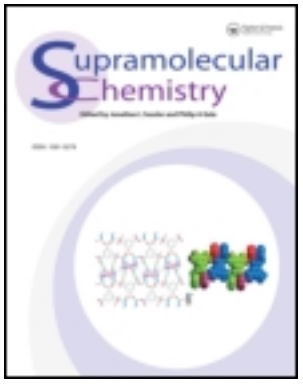

Supramolecular Chemistry
Publication details, including instructions for authors and subscription information:
http://www.tandfonline.com/loi/gsch20

Synthesis and binding investigations of novel crown-ether derivatives of phenanthro[4,5-abc]phenazine and quinoxalino[2′,3′:9,10]phenanthro[4,5-abc]phenazine

Fadi M. Jradi[a], Ala'a O. El-Ballouli[a], Mohammad H. Al-Sayah[b] & Bilal R. Kaafarani[a]
[a] Department of Chemistry, American University of Beirut, Beirut, 1107-2020, Lebanon
[b] Department of Biology, Chemistry and Environmental Sciences, American University of Sharjah, P.O. Box: 26666, Sharjah, United Arab Emirates
Published online: 25 Aug 2013.

To cite this article: Fadi M. Jradi, Ala'a O. El-Ballouli, Mohammad H. Al-Sayah & Bilal R. Kaafarani (2014) Synthesis and binding investigations of novel crown-ether derivatives of phenanthro[4,5-abc]phenazine and quinoxalino[2′,3′:9,10]phenanthro[4,5-abc]phenazine, Supramolecular Chemistry, 26:1, 15-24, DOI: 10.1080/10610278.2013.817577

To link to this article: http://dx.doi.org/10.1080/10610278.2013.817577

Supramolecular Chemistry, 2014
Vol. 26, No. 1, 15–24, http://dx.doi.org/10.1080/10610278.2013.817577

Taylor & Francis
Taylor & Francis Group

Synthesis and binding investigations of novel crown-ether derivatives of phenanthro[4,5-*abc*] phenazine and quinoxalino[2′,3′:9,10]phenanthro[4,5-*abc*]phenazine

Fadi M. Jradi[a], Ala'a O. El-Ballouli[a], Mohammad H. Al-Sayah[b]* and Bilal R. Kaafarani[a]*

[a]*Department of Chemistry, American University of Beirut, Beirut 1107-2020, Lebanon;* [b]*Department of Biology, Chemistry and Environmental Sciences, American University of Sharjah, P.O. Box: 26666, Sharjah, United Arab Emirates*

(*Received 15 April 2013; final version received 13 June 2013*)

The synthesis and binding investigation of novel crown-ether derivatives of phenanthro[4,5-*abc*]phenazine and quinoxalino [2′,3′:9,10]phenanthro[4,5-*abc*]phenazine sensors are reported. The binding studies of these sensors with an array of alkali and alkaline-earth metals are exploited using UV–vis, fluorescence and nuclear magnetic resonance spectroscopies.

Keywords: crown ethers; fluorescent sensors; cation detection, fluoroionophore; spectroscopic titrations; NMR titrations

Introduction

An attractive field of application for fluorophores is their incorporation in the structures of chemical sensors as optical probes to produce colorimetric and fluorescent chemical sensors for neutral and ionic analytes. Such sensors are gaining a lot of attention due to their high sensitivity at low concentration, low cost and ease of application as diagnostic tools (*1*, *2*). In addition, such chemical sensors do not require expensive and laborious analytical techniques and they allow real-time detection. Therefore, there is a major interest in developing new sensors for applications in environmental monitoring, food control and analysis or medical diagnosis and treatment (*3*).

Several recent review articles have addressed the design and main features of fluorescent and colorimetric chemosensors (*3–8*). In general, the molecular design of an optical sensor relies on two major components: (i) the binding site and (ii) the fluorophore. The interaction of an analyte with the binding site triggers electronic changes in the system leading to either emission enhancement or quenching of the fluorescence and/or the absorbance. The selectivity of the sensor depends mainly on the binding site and the molecular recognition components imbedded within its structure. However, the sensitivity of the sensor depends on both the binding efficacy and the corresponding effect of the binding event on the fluorophore's absorbance or emission. The latter relies on the intrinsic properties of the fluorophore (such as quantum yield) and the signalling mechanisms between the binding site and the fluorophore such as photo-induced electron transfer (*9*, *10*), intramolecular charge transfer (ICT) (*10–12*), metal-to-ligand charge transfer (*13*) or excited-state intramolecular proton transfer (*14*).

Phenanthro[4,5-*abc*]phenazine (DPP) and quinoxalino [2′,3′:9,10]phenanthro[4,5-*abc*]phenazine (TQPP) derivatives are large chromophores with high fluorescence quantum yields and interesting opto-electronic properties (*15–33*). These chromophores have recently been established as effective probes in the chemical sensors of anions, such as carboxylates, fluorides and cyanides (*34*). Also, we have reported recently a sensor for metal ions consisting of a TQPP fluorescent core derivatised with crown-ether groups as binding ligands for alkaline and alkali-earth metals (*35*). Crown ethers are known to be effective ligands for Group I and Group II metal ions, and they have been exploited in a wide range of applications such as artificial ion channels (*36*), smart materials (*37*), molecular devices (*38*) and antitumour agents (*39*). These ligands exhibit variable binding modes and selectivity of metal ions based on their size and charge. Here, we report the synthesis and the binding investigations of TQPP- and DPP-based sensors equipped with crown-ether ligands of variable cavity sizes. This report presents the results of spectroscopic and nuclear magnetic resonance (NMR) investigations of sensors **1**–**3** (Scheme 1), shedding light on the binding and the effectiveness of the signalling modes of these sensors upon interaction of the crown ethers with Group I and Group II metal ions. We previously reported the synthesis and binding studies of sensor **4** (*35*) and, recently, we reported the X-ray structure and polymorphism of **2** (*40*).

Results and discussion

The synthesis of sensors **1**–**4** is illustrated in Scheme 1. The intermediates 2,7-di-*tert*-butyldiketopyrene (**7**) and

*Corresponding authors. Email: malsayah@aus.edu; bilal.kaafarani@aub.edu.lb

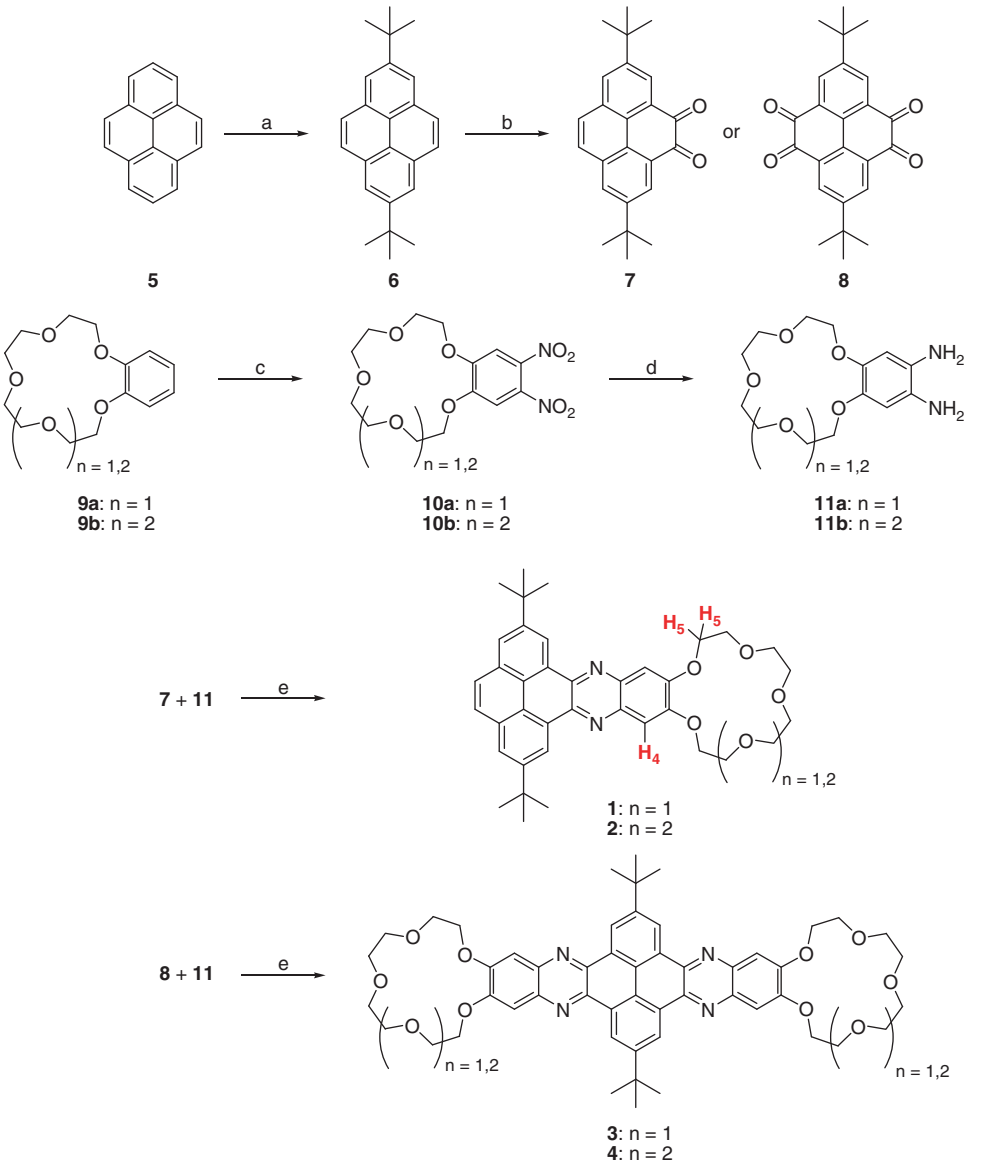

Scheme 1. (Colour online) Synthetic scheme of **1**–**4**. (a) *t*-BuCl, $AlCl_3$; (b) $RuCl_3.xH_2O$, $NaIO_4$, CH_2Cl_2, MeCN, H_2O; (c) HNO_3, $CHCl_3$; (d) H_2 (40 psi), Pd/C, methanol and (e) methanol.

2,7-di-*tert*-butyltetraketopyrene (**8**) were prepared by the catalytic oxidation of di-*tert*-butylpyrene (**6**) using ruthenium(III) chloride and sodium *meta* periodate (*41*). Nitration of the benzocrown **9** with nitric acid in chloroform produced the dinitro product **10**, which upon reduction yielded **11** (*42*). Condensation of **7** and **11** afforded **1** and **2**, whereas the condensation of **8** and **11** yielded **3** and **4**.

Metal effects on absorbance

The detection efficacy of Group I and Group II metal ions by the DPP and TQPP sensors was explored using absorption, emission and NMR spectroscopies, where the spectral changes in the sensors were recorded as metal solutions were introduced at increasing concentrations. The general trends for the binding interactions of 15-crown-5 and 18-crown-6 ethers with Group I and Group II metal ions are well established (*43*), which are based on ion charge and size matching between the ions and the ligand cavities. For example, 15-crown-5 cavity size is best matched by sodium ions, and thus, the binding strengths decrease as follows: $Na^+ > Li^+ > K^+ > Rb^+ > Cs^+$. However, potassium ions best fit inside 18-crown-6 cavity and the binding trend is $K^+ > Na^+ > Rb^+ > Cs^+ > Li^+$, whereas doubly charged ions usually exhibit higher binding affinity to crown ethers than to mono-positive ions with similar sizes (*44*). These trends are

highly affected and altered by several factors such as the type and number of substituents on the crown ether, the counter anions of the metals or the solvent polarity. Therefore, the aim of our study was to explore the ability of molecules **1**–**3** to translate the binding interactions between the ions and the crown ethers into an easily detectable optical signal, and hence, the utility of **1**–**3** as optical sensors for the detection of Group I and Group II metal ions.

The UV–vis spectrum of **1** exhibited the characteristic peaks of a DPP chromophore at 280, 355 and 440 nm (Figure 1). The addition of alkaline and alkali-earth metal ions to **1** led to an increase in absorbance at 280 nm and to diminished absorbance at 305 and 440 nm concomitant with the appearance of several isosbestic points at 305, 330, 405 and 450 nm. This behaviour indicates the strong binding interaction between the sensor and the metal ions. Figure 1 illustrates the changes observed in the absorption spectra of **1** (1.0 μM in 1:1 CH_2Cl_2:CH_3CN) upon titrating it with solutions of calcium ions (1 mM in 1:1 CH_2Cl_2:CH_3CN).

The different metal–sensor interactions were demonstrated through the relative changes in the absorbance of **1**. Figure 2 exhibits the effect of each metal ion on the absorbance intensity of **1** at 438 nm. This graph indicates that doubly charged ions have the most significant effect on absorbance, which decreases by ~25% upon addition of ~5 molar equivalents of the ions. The effect of mono-charged metal ions on absorbance of **1** generally correlates with the binding trend of the ions to 15-crown-5 ligand which reflects the size matching between metal ions and the ligand cavity ($Na^+ > Li^+ > K^+ > Rb^+ > Cs^+$) (*44*). These results indicate that the change in the absorbance signal of sensor **1** follows the actual trend of binding strength of these metal ions to the crown ether.

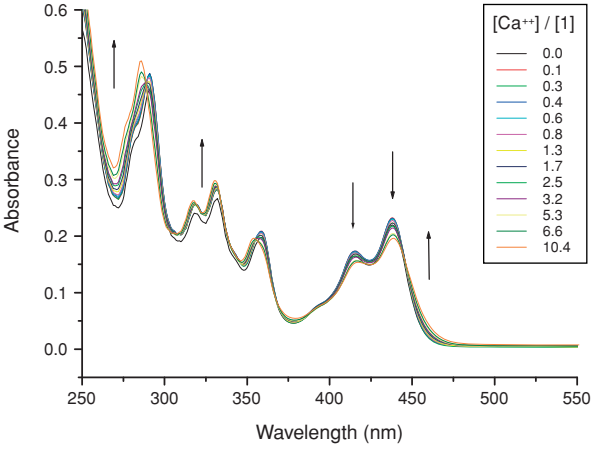

Figure 1. (Colour online) UV–vis spectra of **1** (1.0 μM) upon titration with solutions of calcium ions (0.1 mM) in 1:1 CH_2Cl_2:CH_3CN.

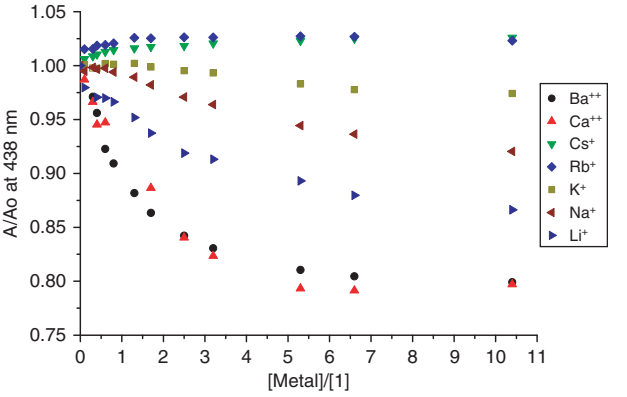

Figure 2. (Colour online) Relative change (A/A_o) in the absorbance of **1** (1.0 μM) at 438 nm upon titration with solutions of different metal ions (0.1 mM) in 1:1 CH_2Cl_2:CH_3CN.

The absorbance spectrum of sensor **2** exhibits the same characteristic peaks related to the DPP chromophore at 280, 355 and 440 nm (Figure 3). The addition of metal ions to **2** leads to an increase in the absorbance at 280 nm and to a diminished absorbance at 305 and 440 nm concomitant with several isosbestic points at 305, 330, 405 and 450 nm. The changes observed in the absorption spectra of **2** (1.0 μM in 1:1 CH_2Cl_2:CH_3CN), upon titration with a solution of the metal ions (0.1 mM in 1:1 CH_2Cl_2:CH_3CN), are similar to those of sensor **1** and are attributed to the binding interactions between the sensor and the metal ions. By comparing the relative effects of all ions on the absorbance of **2** (Figure 4), it can be noted that the binding trend (*43*, *44*) for 18-crown-6 with the metal ions is reflected by the changes in the absorbance of **2**.

The absorbance spectrum of sensor **3** exhibits the characteristic peaks of the TQPP chromophore (*34*, *35*) at 285, 400 and 425 nm (Figure 5). Similar to **1** and **2**, the addition of metal ions to a solution of **3** results in spectral

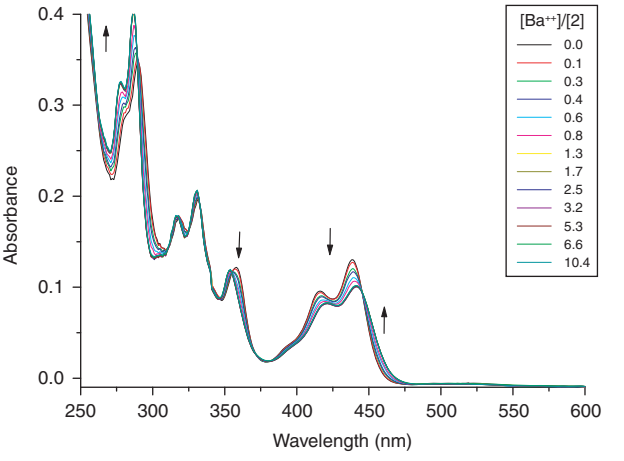

Figure 3. (Colour online) UV–vis spectra of **2** (1.0 μM) upon titration with solutions of barium ions (0.1 mM) in 1:1 CH_2Cl_2:CH_3CN.

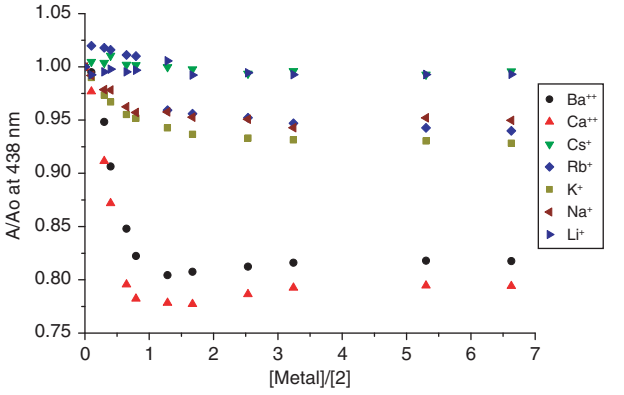

Figure 4. (Colour online) Relative change (A/A_o) in the absorbance of **2** (1.0 μM) at 438 nm upon titration with solutions of different metal ions (0.1 mM) in 1:1 CH_2Cl_2:CH_3CN.

changes in the latter as demonstrated in Figure 5 for the addition of calcium ions. Sensor **3** (1.0 μM in 1:1 CH_2Cl_2:CH_3CN) experiences increased absorbance at 285 nm and diminished absorbance at 400 and 425 nm in parallel with several isosbestic points at 280, 325, 343 and 440 nm upon titrating with calcium ions (0.1 mM in 1:1 CH_2Cl_2:CH_3CN).

Similar to **1**, relative change in absorbance of **3** at 425 nm upon addition of the metal ions (Figure 6) reflects expected trend of binding of the metal ions to 15-crown-5 ether with regard to doubly charged ions (*43*, *44*). Barium and calcium ions, for example, show the most significant impact on absorbance, which decreased by ~20% upon the addition of ~20 molar equivalents of the ions. This sensor is expected to bind to these metal ions with two molecules in a 'sandwich' confirmation (*vide infra*) as was noted earlier for **4** (*35*, *44*). Nonetheless, the effect of the mono-charged metal ions correlates with the binding trend of the 15-crown-5 ether and the observed trend of **1** with these ions.

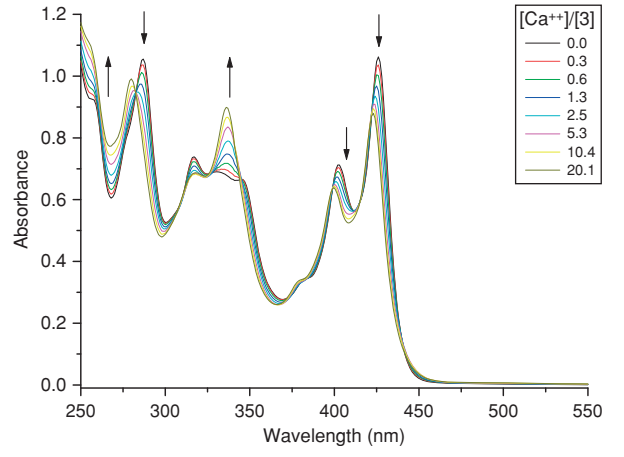

Figure 5. (Colour online) UV–vis spectra of **3** (1.0 μM) upon titration with solutions of calcium ions (0.1 mM) in 1:1 CH_2Cl_2:CH_3CN.

Metal effects on emission

The effect of the metal ions on the emission of **1**–**3** was also studied to determine the utility of these molecules as fluorescent sensors. Sensors **1** and **2** exhibit maximum emission at 470 nm upon excitation at 350 nm in 1:1 CH_2Cl_2:CH_3CN. The addition of doubly charged metal ions leads to lower emission of both sensors with a bathochromic shift of the emission maximum by about 10 nm after the addition of ~2 molar equivalents for **1** and 5 molar equivalents for **2** of barium or calcium ions (Figure 7). Further addition of these ions has no significant effect on the emission. Addition of the singly charged alkali metal ions to either sensors (**1** or **2**) results in fluorescence quenching with no bathochromic shift of the 470 nm emission maximum. The quenching effect decreases in going down the group, which reflects a similar trend of effect as observed on the absorbance signal for both sensors (*vide supra*). This quenching effect of metal ions on **1** and **2** is attributed to the inhibition of ICT between the crown and the aromatic fluorophore upon binding of the positively charged ions to the crowns.

The emission of sensor **3** and the influence of ions on its emission are slightly different from those of **1** and **2** due to the extended chromophore and the presence of two crown-ether ligands (Figure 8). Sensor **3** exhibits a strong emission with a maximum at 450 nm upon excitation at 350 nm. Addition of the divalent ions (barium and calcium) results in quenching and slight bathochromic shift (~10 nm) of the emission at 450 nm and enhancement of the emission at 550 nm. Monovalent alkali metal ions cause only a reduction in emission with no major shift in emission maximum. The change in the emission intensity of **3** reflects the expected binding interaction strength between the benzo-15-crown-5 and Group I ions, in which sodium ions have the highest effect ($Na^+ > Li^+ > K^+ > Rb^+ > Cs^+$).

NMR studies of metal effects

To shed more light on the mode of interactions of the sensors with the metal ions, NMR studies were conducted on the sensors in the presence of variable concentrations of the metal ions. The addition of the metal ions to sensors **1** and **2** in $CDCl_3$:CD_3CN (1:1) (sensor **3** has a low solubility) results in significant changes in the chemical shifts of the crown-ether protons and the aromatic chromophore. Specifically, the chemical shifts of the H_4 and H_5 protons (Scheme 1) were monitored upon the addition of the metal ions at increasing concentrations. In general, the addition of the metal ions leads to downfield shift in the chemical shift of H_5 (Figure 9) due to the binding of O-atoms of the crown ether with the positively charged metal ions. The stronger the binding and the higher the charge density, the larger the shift.

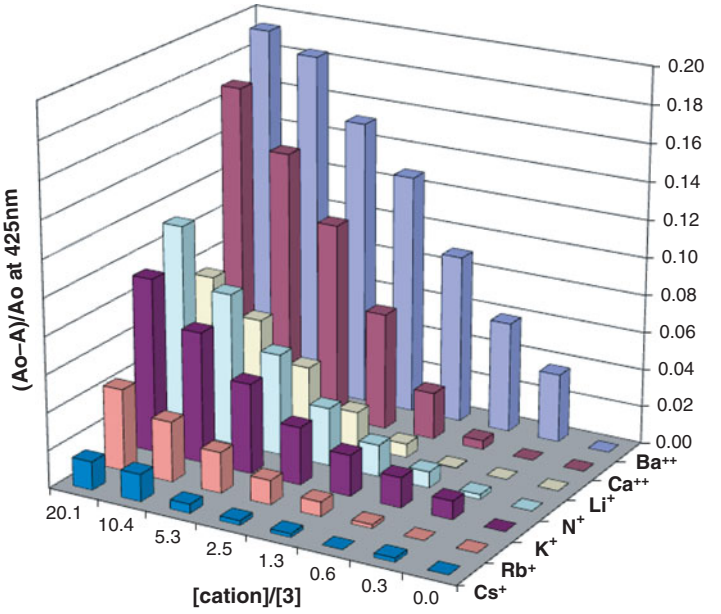

Figure 6. (Colour online) Normalised change ($A_o - A/A_o$) in the absorbance of **3** (1.0 μM) at 425 nm upon titration with solutions of different metal ions (0.1 mM) in 1:1 CH_2Cl_2:CH_3CN.

In general, the change in the chemical shift of H_5 protons reflects the binding trend (observed earlier) of the crown with these metals, in which the most significant shift was observed upon addition of the doubly charged ions (barium and calcium). After the addition of 1.0 molar equivalent of each metal, no further significant downfield shift was observed for these protons (Figure 9). This implies that the crown becomes saturated with the metal after addition of 1 molar equivalent, which suggests a 1:1 binding stoichiometry. Meanwhile, singly charged ions exhibit lower effects on the crown-ether protons (H_5), but correlate with ion-crown size matching (*44*). Sodium ions result in the most significant shift and as the size of the ion increases (in going to potassium, rubidium and cesium), the shift in the chemical shift of the crown's protons decreases reflecting the decrease in charge concentration on the ion.

The effect of the ion size on the binding mode of **1** is more evident when analysing the changes in the signal of the aromatic protons H_4, for which trends are different with respect to H_5 (Figure 10). The binding of the metal ions leads to downfield shift of the aromatic protons (H_4) of the ring that is directly attached to the crown-ether ligand. This trend is observed upon the addition of calcium and sodium ions, which have similar sizes and are the best fit to bind inside the crown-ether cavity of sensor **1** with 1:1 binding ratio (Figure 10). The addition of barium, potassium and, to a lower extent, rubidium ions to the sensor results initially in upfield shift in the signals of H_4

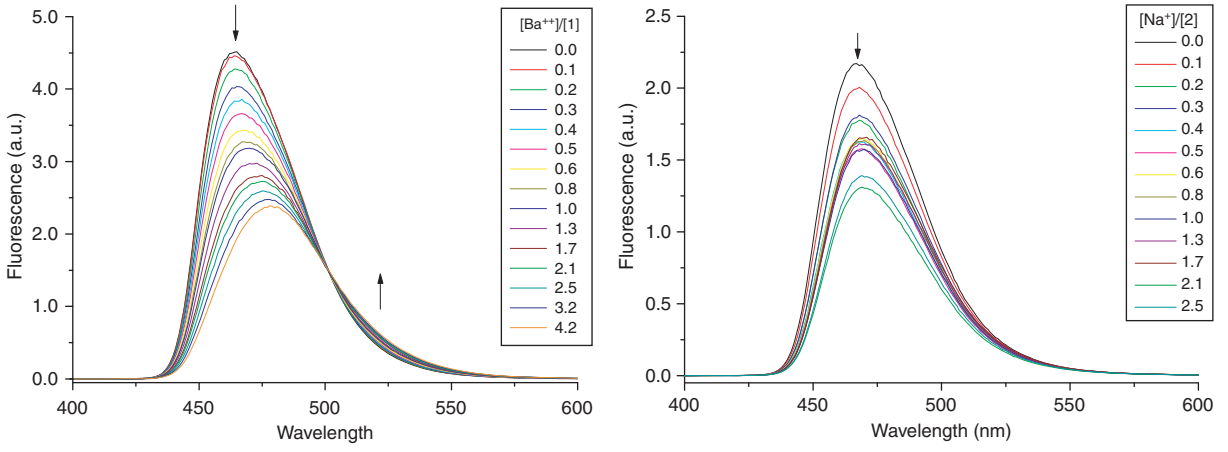

Figure 7. (Colour online) Emission spectra (λ_{ex} = 350 nm) of **1** (left) and **2** (right) (1.0 μM) upon titration with solutions (0.1 mM) of barium and sodium ions, respectively, in 1:1 CH_2Cl_2:CH_3CN.

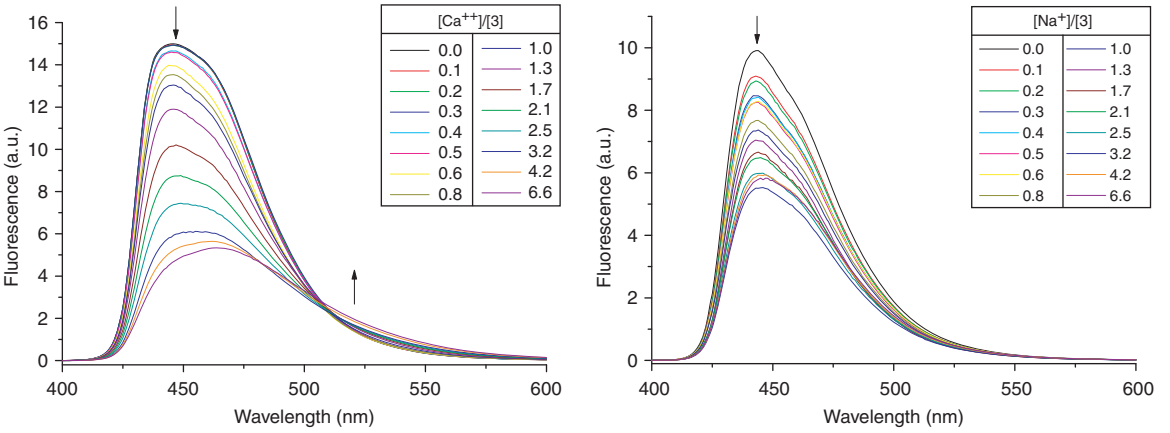

Figure 8. (Colour online) Emission spectra ($\lambda_{ex} = 350$ nm) of **3** (1.0 μM) upon titration with solutions (0.1 mM) of calcium (left) and sodium (right) ions in 1:1 CH_2Cl_2:CH_3CN.

until 0.5 molar equivalent of the metal ion is added. Then, as more ions are added, the signals of H_4 shift downfield up to 2 molar equivalents. These results indicate that the large-size ions (barium, potassium and rubidium) require two crown ethers to bind to each ion resulting in a 'sandwich' metal-complex configuration (Figure 11). Such a configuration, which is favourable once <0.5 molar equivalent of the metal ion is added, places the aromatic protons of one ring in the shielding cone of the other ring resulting in an upfield shift of the H_4 protons overcoming the downfield shift caused by the electrostatic effect of the metal ions. As more metal ions are added, the 2:1 complex starts to break apart to form 1:1 complex of sensor **1** and the metal, hence the downfield shift of the H_4 signal. Cesium ions are too large to show any significant binding with 15-crown-5 ligand. Finally, although lithium ions are too small to bind tightly inside the cavity of 15-crown-5, at high concentration, the binding equilibrium shifts towards the formation of the complex resulting in a downfield shift of the signal of H_5 protons and, to more extent, of H_4 protons. The large charge density and the size mismatch of lithium ion with the crown cause the ion to bind with the pre-organised and the less flexible binding site provided by the two O-atoms attached to the π-system and away from the centre of the crown. This close proximity to the π-system (*45*) and to H_4 leads to the larger downfield shift of the aromatic H_4 protons as compared with H_5.

The binding constant of each ion with **1** and **2** was estimated (Table 1) using the binding isotherms shown earlier (Figures 9 and 10). The calculations take into consideration the equilibria, which are associated with forming and breaking the 'sandwich' complex of **1** with barium, rubidium and potassium ions in which good fit was obtained with the model combining the equilibrium 2:1 with 1:1 sensor–ion complex. The binding isotherms of the remaining ions generated a good fit to a 1:1 binding model, which was also applied to the binding isotherms of sensor **2** with all ions (See Supporting Information for further details, available online).

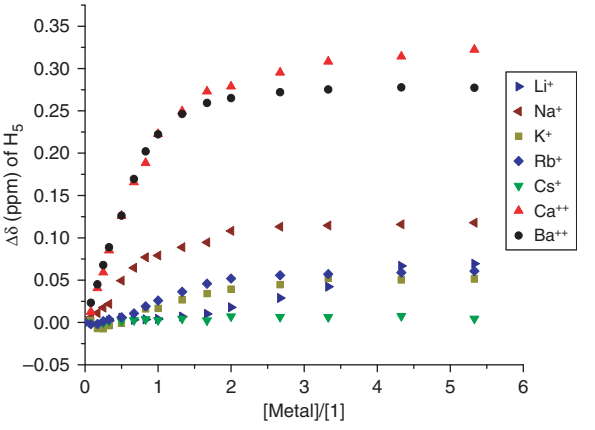

Figure 9. (Colour online) The change (Δδ) in the chemical shift of H_5 of **1** (2.0 mM) upon titration with solutions of different metal ions (10 mM) in 1:1 $CDCl_3$:CD_3CN.

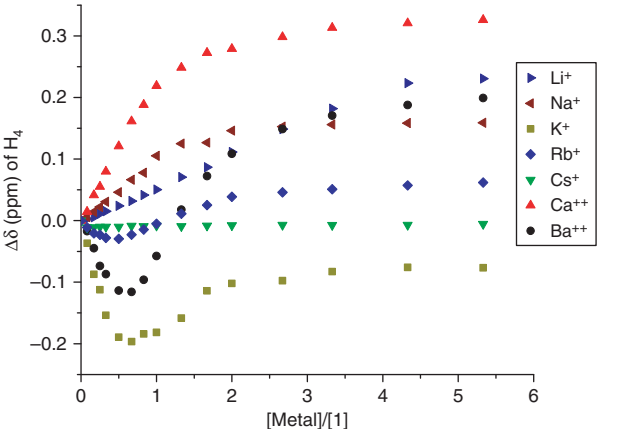

Figure 10. (Colour online) The change (Δδ) in the chemical shift of H_4 of **1** (2.0 mM) upon titration with solutions of different metal ions (10 mM) in 1:1 $CDCl_3$:CD_3CN.

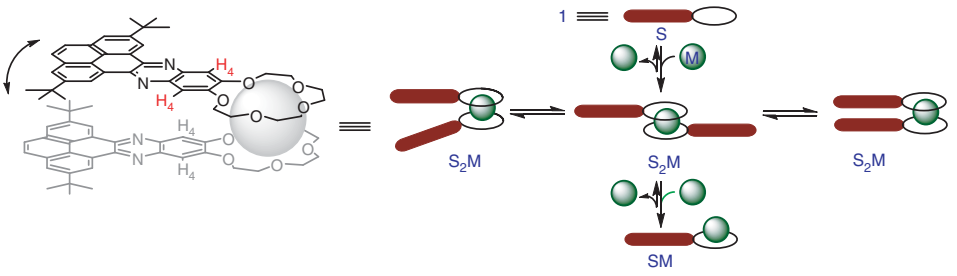

Figure 11. (Colour online) Schematic representation of the 'sandwich' complex of sensor **1** with barium, potassium and rubidium ions.

Sensor **2**, however, exhibits a trend different from **1** in its binding mode to the metals. The change in the chemical shift of crown-ether protons (H_5) shows (Figure 12) a downfield shift upon addition of the metal ions, which reaches a maximum after ~1.0 molar equivalence. However, as the size of crown is bigger, the highest effect is for barium. The potassium ion, which has a size very similar to barium (*44*), displays the highest downfield shift among the monovalent ions. This reflects the effect of the crown size on the binding efficacy of the sensors with the metals.

This size effect of the crown in sensor **2** is further supported by the changes in the chemical shift of the aromatic protons (H_4) (Figure 13). The signal of the H_4 protons of **2** shifted only downfield upon addition of barium and potassium ions. This is attributed to the large cavity size of the 18-crown-6, which is able to accommodate these ions mainly inside the pocket, which makes the metal closer to the H_4 protons. This close proximity increases the through–space interactions between the metal ions and H_4 protons, which results in downfield shift reflecting the absence of the sandwich conformation noted with **1** and the formation of 1:1 complex. Finally, similar to **1**, the large downfield shift observed for H_4 protons upon addition of large amounts of lithium and sodium ions can be attributed to the large charge density and the size mismatch of these ions with the crown, which lead them to bind close to the π-system away from the centre of the crown.

Conclusions

The spectroscopic investigations of the interaction of the sensors with the metal ions have shown that the changes in either absorption or emission reflect the correct order and strength of crown–ions interactions. However, the mode and the stoichiometry of binding were better reflected through NMR binding investigations. Sensor **1** forms 1:1 complexes with small ions (sodium and calcium) and 1:2 complexes with large ions (potassium, rubidium, cesium and barium) as evidenced by the changes in the chemical shifts of the H_4 and H_5 protons. Sensor **2** shows weak binding with small monovalent ions (lithium and sodium) but it forms 1:1 complexes with calcium, potassium and barium ions. Finally, absorbance and emission studies indicate strong binding to barium and calcium ions with **3**; however, it was not possible to confirm the exact mode of binding of **3** to the metals by NMR studies due to its low solubility.

Experimental

Synthesis

Chemicals and solvents were purchased from Acros, Geel, Belgium. Standard grade silica gel (60 Å, 32–63 μm) and silica gel plates (200 μm) were purchased from Sorbent Technologies, Atlanta, GA, USA. Reactions that required anhydrous conditions were carried out under argon in oven-dried glassware. A Bruker Avance 300 NMR spectrometer (wide bore) was used to record the NMR spectra. $CDCl_3$ was the solvent for NMR measurements, and chemical shifts relative to tetramethylsilane (TMS) at 0.00 ppm are reported in ppm on the δ scale. The MALDI data were acquired at the Bioanalytical Mass Spectrometry Facility at the Georgia Institute of Technology, Atlanta, GA, USA.

2,7-Di-*tert*-butylpyrene-4,5-dione (**7**) (*41*), 2,7-di-*tert*-butylpyrene-4,5,9,10-tetraone (**8**) (*41*), 1,2-diamino-benzo-15-crown-5 (**11a**) (*42*) and 2,3-dinitro-benzo-18-crown-6 (**11b**) (*42*) were synthesised according to literature procedures.

Table 1. Binding constants of sensors **1** and **2** to the cations.

	Ion radius (Å)[a]	Li^+(0.76)	Na^+(1.02)	K^+(1.38)	Rb^+(1.52)	Cs^+(1.67)	Ca^{++}(1.00)	Ba^{++}(1.35)
1	Log K_1[b] (M^{-1})	<2[c]	3.4	3.6	3.4	< 2[c]	3.4	4.3
	Log K_2[b] (M^{-2})	–		>6	4.8	–	–	>6
2	Log K_1[b] (M^{-1})	<2[c]	<2[c]	4.3	<2[c]	<2[c]	>6	>6

[a] Data from Ref. (*44*).
[b] Calculated from the change in the chemical shifts of H_5 upon titrating with the metals.
[c] The binding isotherm did not fit to the binding model due to low association constant. More details in Supporting Information, available online.

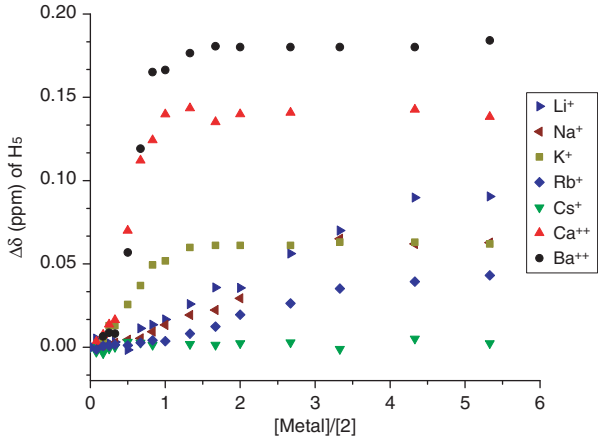

Figure 12. (Colour online) Change ($\Delta\delta$) in the chemical shift of H_5 of **2** (2.0 mM) upon titration with solutions of different metal ions (10 mM) in 1:1 $CDCl_3$:CD_3CN.

*2,7-Bis(1,1-dimethylethyl)-12,13,15,16,18,19,21,22-octahydro-[1,4,7,10,13]pentaoxacyclopentadecino[2,3-*i*]phenanthro[4,5-*abc*]phenazine (**1**)*

1,2-Diamino-benzo-15-crown-5 (**11a**) (1.00 g, 3.35 mmol) was added to a solution of 2,7-di-*tert*-butylpyrene-4,5-dione (**7**) (1.15 g, 3.35 mmol) in 300 ml of methanol, and the reaction mixture was refluxed for 48 h. The final yellow product was filtered and washed with copious amount of methanol to afford **1** (1.20 g, 60%). ^{1}H NMR (300 MHz, $CDCl_3$): δ 1.66 (18H, s), 3.85 (8H, s), 4.07 (4H, t, $J = 3.9$ Hz), 4.44 (4H, t, $J = 2.4$ Hz), 7.62 (2H, s), 8.00 (2H, s), 8.25 (2H, d, $J = 1.8$ Hz), 9.60 (2H, d, $J = 1.8$ Hz). ^{13}C NMR (75 MHz, $CDCl_3$): δ 31.93, 35.53, 68.43, 69.04, 70.12, 71.25, 107.13, 120.46, 123.76, 124.92, 127.26, 129.21, 131.09, 139.87, 141.41, 149.43, 152.84. HRMS-MALDI (*m/z*): $[M + H]^+$: calculated for $C_{38}H_{43}N_2O_5$, 607.3166; Found, 607.3212.

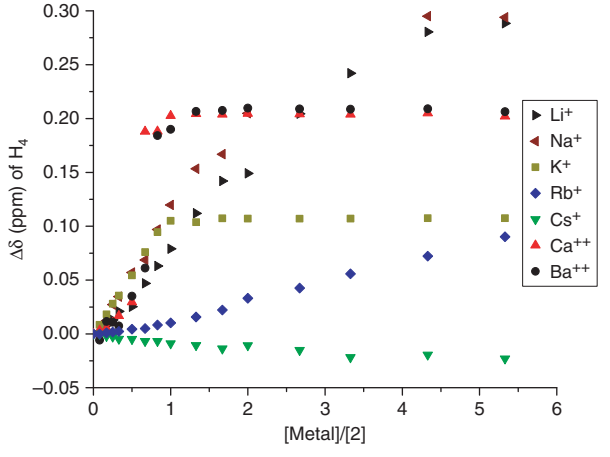

Figure 13. (Colour online) Change ($\Delta\delta$) in the chemical shift of H_4 of **2** (2.0 mM) upon titration with solutions of different metal ions (10 mM) in 1:1 $CDCl_3$:CD_3CN.

*2,7-Bis(1,1-dimethylethyl)-12,13,15,16,18,19,21,22,24,25-decahydro-[1,4,7,10,13,16]hexaoxacyclooctadecino[2,3-*i*]phenanthro[4,5-*abc*]phenazine (**2**)*

2,3-Dinitro-benzo-18-crown-6 (**11b**) (0.50 g, 1.68 mmol) was added to a solution of 2,7-di-*tert*-butylpyrene-4,5-dione (**7**) (0.50 g, 1.45 mmol) in 250 ml of methanol, and the reaction mixture was refluxed for 48 h. The final yellow product was filtered and washed with copious amount of methanol to afford **2** (1.20 g, 60%). ^{1}H NMR (300 MHz, $CDCl_3$): δ 1.69 (18H, s), 3.74 (4H, s), 3.77 (4H, t, $J = 3.9$ Hz), 3.86 (4H, t, $J = 3.1$ Hz), 4.093 (4H, t, $J = 3.9$ Hz), 4.42 (4H, t, $J = 3.6$ Hz), 7.34 (2H, s), 8.00 (2H, s), 8.25 (2H, d, $J = 1.8$ Hz), 9.60 (2H, s). ^{13}C NMR (75 MHz, $CDCl_3$): δ 31.59, 35.53, 69.00, 69.14, 70.50, 70.77, 71.02, 107.11, 120.46, 123.75, 124.93, 127.26, 129.21, 131.08, 139.79, 141.44, 149.43, 152.77. HRMS-MALDI (*m/z*): $[M + H]^+$: calculated for $C_{40}H_{47}N_2O_6$, 651.3429; Found, 651.3411.

*2,22-Bis(1,1-dimethylethyl)-7,8,10,11,13,14,16,17,27,28,30,31,33,34,36,37-hexadecahydro-[1,4,7,10,13]pentaoxacyclopentadecino[2″,3″:6′,7′]quinoxalino[2′,3′:9,10]phenanthro[4,5-*abc*][1,4,7,10,13]pentaoxacyclopentadecino[2,3-*i*]phenazine (3)*

1,2-Diamino-benzo-15-crown-5 (**11a**) (0.83 g, 2.79 mmol) was added to a solution of 2,7-di-*tert*-butylpyrene-4,5,9,10-tetraone (8) (0.52 g, 1.39 mmol) in 300 ml of methanol, and the reaction was refluxed for 48 h. The compound was filtered and washed with copious amount of methanol to afford 3 (1.20 g, 50%). ^{1}H NMR (300 MHz, $CDCl_3$): δ 1.75 (18H, s), 3.85 (8H, s), 4.07 (4H, t, $J = 3.9$ Hz), 4.44 (4H, t, $J = 2.4$ Hz), 7.61 (2H, s), 9.72 (2H, s). Analysis calculated for $C_{52}H_{58}N_4O_{10}$: C, 69.47; H, 6.50: N, 6.23.Found: C, 69.28; H, 6.46; N, 6.04.HRMS-MALDI (*m/z*): $[M + H]^+$: calculated for $C_{52}H_{59}N_4O_{10}$, 899.4226; Found, 899.4268.

Spectroscopic titration

A solution of the sensor (1 μM, 2 ml) in CH_2Cl_2:CH_3CN (1:1) placed into a 1 cm × 1 cm cuvette was titrated with a solution of the metal ion [0.1 mM, CH_2Cl_2:CH_3CN (1:1)] that contained the sensor (1 μM). Aliquot amounts of the metal ion solution were added to the cuvette via a syringe until a total of six or more equivalents of the metal ion had been added (the number of additions was around 20 with an increase in the amount of metal ion solution added). The UV–vis spectrum and emission spectrum ($\lambda_{ex} = 350$ nm) were scanned after each addition.

^{1}H NMR Titration

A solution of the sensor (2 mM, 600 μl) in $CDCl_3$:CD_3CN (1:1) placed in an NMR tube was titrated with a solution of the metal ion (10 mM). Aliquot amounts of the metal ion solution were added to the NMR tube via a syringe until a total of 10 equivalents of the metal ion were added (the number of additions was around 17 with an increase in the amount of metal ion solution added). An ^{1}H NMR spectrum was recorded after each addition, and the chemical shifts of the aromatic protons were recorded. The collected data were analysed using a nonlinear least square regression programme to fit the data to a theoretical model of 1:1 for sensors **1** and **2** and 1:2 for sensor **3**.

Supplemental Information

UV–vis, fluorescence, NMR titrations, calculations of binding constants and fitting of binding isotherms of **1**–**3** are provided in the Supporting Information. This information is available free of charge at http://www.tandfonline.com/.

Acknowledgements

The authors thank Prof. Jean-Luc Brédas, Prof. Tarek Ghaddar, Prof. Brigitte Wex and Dr Veaceslav Coropceanu for insightful discussions. This work was supported by the Lebanese National Council for Research (CNRS) and the American University of Sharjah (Grants: FRG08-2-01 and FRG12-3-18). The authors are grateful for this support.

References

(1) Hertzog-Ronen, C.; Borzin, E.; Gerchikov, Y.; Tessler, N.; Eichen, Y. *Chem. Eur. J.* **2009**, *15*, 10380–10386.
(2) Lee, K.-S.; Kim, H.-J.; Kim, G.-H.; Shin, I.; Hong, J.-I. *Org. Lett.* **2008**, *10*, 49–51.
(3) Lodeiro, C.; Capelo, J.L.; Mejuto, J.C.; Oliveira, E.; Santos, H.M.; Pedras, B.; Nunez, C. *Chem. Soc. Rev.* **2010**, *39*, 2948–2976.
(4) Tsukanov, A.V.; Dubonosov, A.D.; Bren, V.A.; Minkin, V. I. *Chem. Heterocycl. Compd.* **2008**, *44*, 899–923.
(5) Bell, T.W.; Hext, N.M. *Chem. Soc. Rev.* **2004**, *33*, 589–598.
(6) Leray, I.; Valeur, B. *Eur. J. Inorg. Chem.* **2009**, 3525–3535.
(7) Fery-Forgues, S.; Al-Ali, F. *J. Photochem. Photobiol. C* **2004**, *5*, 139–153.
(8) Kim, S.K.; Lee, D.H.; Hong, J.-I.; Yoon, J. *Acc. Chem. Res.* **2009**, *42*, 23–31.
(9) Gunnlaugsson, T.; Davis, A.P.; O'Brien, J.E.; Glynn, M. *Org. Biomol. Chem.* **2005**, *3*, 48–56.
(10) Gunnlaugsson, T.; Kruger, P.E.; Lee, T.C.; Parkesh, R.; Pfeffer, F.M.; Hussey, G.M. *Tetrahedron Lett.* **2003**, *44*, 6575–6578.
(11) Bernard, V. *Molecular Fluorescence: Principles and Applications*; Wiley-VCH: Hoboken, NJ, 2001.
(12) Wen, Z.-C.; Jiang, Y.-B. *Tetrahedron* **2004**, *60*, 11109–11115.
(13) Atkinson, P.; Bretonniere, Y.; Parker, D. *Chem. Commun.* **2004**, 438–439.
(14) Zhao, L.; YaoHan, C.; YunBao, J. *Sci. China Ser. B-Chem.* **2009**, *52*, 786–792.
(15) Bon, S.B.; Valentini, L.; Moustafa, R.M.; Jradi, F.M.; Kaafarani, B.R.; Verdejo, R.; Lopez-Manchado, M.A.; Kenny, J.M. *J. Phys. Chem. C* **2010**, *114*, 11252–11257.
(16) Leng, S.; Chan, L.H.; Jing, J.; Hu, J.; Moustafa, R.M.; Van Horn, R.M.; Graham, M.J.; Sun, B.; Zhu, M.; Jeong, K.-U.; Kaafarani, B.R.; Zhang, W.; Harris, F.W. *Cheng, S.Z.D. Soft Matter* **2010**, *6*, 100–112.
(17) Leng, S.; Wex, B.; Chan, L.H.; Graham, M.J.; Jin, S.; Jing, A.J.; Jeong, K.-U.; Van Horn, R.M.; Sun, B.; Zhu, M.; Kaafarani, B.R.; Cheng, S.Z.D. *J. Phys. Chem. B* **2009**, *113*, 5403–5411.
(18) Moustafa, R.M.; Degheili, J.A.; Patra, D.; Kaafarani, B.R. *J. Phys. Chem. A* **2009**, *113*, 1235–1243.
(19) Degheili, J.A.; Moustafa, R.M.; Patra, D.; Kaafarani, B.R. *J. Phys. Chem. A* **2009**, *113*, 1244–1249.
(20) Lucas, L.A.; De Longchamp, D.M.; Richter, L.J.; Kline, R. J.; Fischer, D.A.; Kaafarani, B.R.; Jabbour, G.E. *Chem. Mater.* **2008**, *20*, 5743–5749.
(21) Kaafarani, B.R.; Lucas, L.A.; Wex, B.; Jabbour, G.E. *Tetrahedron Lett.* **2007**, *48*, 5995–5998.
(22) Jang, K.; Ranasinghe, A.D.; Heske, C.; Lee, D.-C. *Langmuir* **2010**, *26*, 13630–13636.
(23) Wang, M.; Tong, H.; Cheng, Y.; Xie, Z.; Wang, L.; Jing, X.; Wang, F. *J. Polym. Sci. Part A Polym. Chem.* **2010**, *48*, 1990–1999.
(24) Luo, M.; Shadnia, H.; Qian, G.; Du, X.; Yu, D.; Ma, D.; Wright, J.S.; Wang, Z.Y. *Chem. Eur. J.* **2009**, *15*, 8902–8908.
(25) Margraf, D.; Cekan, P.; Prisner, T.F.; Sigurdsson, S.T.; Schiemann, O. *Phys. Chem. Chem. Phys.* **2009**, *11*, 6708–6714.
(26) Jang, K.; Kinyanjui, J.M.; Hatchett, D.W.; Lee, D.-C. *Chem. Mater.* **2009**, *21*, 2070–2076.
(27) McGrath, K.K.; Jang, K.; Robins, K.A.; Lee, D.-C. *Chem. Eur. J.* **2009**, *15*, 4070–4077.
(28) Schiemann, O.; Cekan, P.; Margraf, D.; Prisner, T.F.; Sigurdsson, S.T. *Angew. Chem. Int. Ed.* **2009**, *48*, 3292–3295.
(29) Wohlthat, S.; Pauly, F.; Reimers, J.R. *J. Phys. Condens. Matter* **2008**, *20*, 295208/1–295208/5.
(30) Lee, D.-C.; McGrath, K.K.; Jang, K. *Chem. Commun.* **2008**, 3636–3638.
(31) Gao, B.; Wang, M.; Cheng, Y.; Wang, L.; Jing, X.; Wang, F. *J. Am. Chem. Soc.* **2008**, *130*, 8297–8306.
(32) Lee, D.-C.; Jang, K.; McGrath, K.K.; Uy, R.; Robins, K.A.; Hatchett, D.W. *Chem. Mater.* **2008**, *20*, 3688–3695.
(33) Hu, J.; Zhang, D.; Jin, S.; Cheng, S.Z.D.; Harris, F.W. *Chem. Mater.* **2004**, *16*, 4912–4915.
(34) Raad, F.S.; El-Ballouli, A.O.; Moustafa, R.M.; Al-Sayah, M.H.; Kaafarani, B.R. *Tetrahedron* **2010**, *66*, 2944–2952.
(35) Jradi, F.M.; Al-Sayah, M.H.; Kaafarani, B.R. *Tetrahedron Lett.* **2008**, *49*, 238–242.
(36) Biron, E.; Otis, F.; Meillon, J.-C.; Robitaille, M.; Lamothe, J.; Van Hove, P.; Cormier, M.-E.; Voyer, N. *Bioorg. Med. Chem.* **2004**, *12*, 1279–1290.
(37) Yagai, S.; Kitamura, A. *Chem. Soc. Rev.* **2008**, *37*, 1520–1529.
(38) Kinbara, K.; Aida, T. *Chem. Rev.* **2005**, *105*, 1377–1400.
(39) Kralj, M.; Tusek-Bozic, L.; Frkanec, L. *ChemMedChem* **2008**, *3*, 1478–1492.

(40) Fonari, A.; Jradi, F.M.; Fonari, M.S.; Al-Sayah, M.H.; Antipin, M.Y.; Kaafarani, B.R.; Timofeeva, T.V. *J. Mol. Struct.* **2011**, *996*, 141–147.
(41) Hu, J.; Zhang, D.; Harris, F.W. *J. Org. Chem.* **2005**, *70*, 707–708.
(42) Pike, J.D.; Rosa, D.T.; Coucouvanis, D. *Eur. J. Inorg. Chem.* **2001**, 761–777.
(43) Arnaud-Neu, F.; Delgado, R.; Chaves, S. *Pure Appl. Chem.* **2003**, *75*, 71–102.
(44) Izatt, R.M.; Bradshaw, J.S.; Nielsen, S.A.; Lamb, J.D.; Christensen, J. *Chem. Rev.* **1985**, *85*, 271–339.
(45) Wheeler, S.E.; Houk, K.N. *J. Am. Chem. Soc.* **2009**, *131*, 3126–3127.